The role of different reorganization energies within the Zusman theory of electron transfer

Cite as: J. Chem. Phys. **118**, 291 (2003); https://doi.org/10.1063/1.1525799
Submitted: 05 August 2002 . Accepted: 07 October 2002 . Published Online: 16 December 2002

Jesús Casado-Pascual, Manuel Morillo, Igor Goychuk, and Peter Hänggi

The role of different reorganization energies within the Zusman theory of electron transfer

Jesús Casado-Pascual and Manuel Morillo
Física Teórica, Universidad de Sevilla, Apartado de Correos 1065, Sevilla 41080, Spain

Igor Goychuk and Peter Hänggi
Institut für Physik, Universität Augsburg, Universitätsstraße 1, D-86135, Augsburg, Germany

(Received 5 August 2002; accepted 7 October 2002)

We consider the kinetics of electron transfer reactions in condensed media with different reorganization energies for the forward and backward processes. The starting point of our analysis is an extension of the well-known Zusman equations to the case of parabolic diabatic curves with different curvatures. A generalized master equation for the populations as well as formal expressions for their long-time limit is derived. We discuss the conditions under which the time evolution of the populations of reactants and products can be described at all times by a single exponential law. In the limit of very small tunnel splitting, a novel rate formula for the nonadiabatic transitions is obtained. It generalizes previous results derived within the contact approximation. For larger values of the tunnel splitting, we make use of the consecutive step approximation leading to a rate formula that bridges between the nonadiabatic and solvent-controlled adiabatic regimes. Finally, the analytical predictions for the long-time populations and for the rate constant are tested against precise numerical solutions of the starting set of partial differential equations. © *2003 American Institute of Physics.* [DOI: 10.1063/1.1525799]

I. INTRODUCTION

Electron transfer reactions are of prime importance in many physicochemical and biological processes.[1] At a very fundamental level, an electron transfer step is essentially an electron tunneling event in the presence of a medium (solvent). A non-negligible tunneling probability requires resonance in the energy of localized electronic states. The solvent thermal fluctuations provide the necessary energy for the resonance condition. Thus, the kinetics of electron transfer reaction requires an adequate description of the medium thermal fluctuations that mediate the electronic charge redistribution in an electron transfer.[2]

In the classical theory of Marcus,[3] Hush,[4] and Levich and Dogonadze[5] the solvent fluctuations are described by an equilibrium probability law. Thus, the knowledge of the free energy as a function of an appropriate reaction coordinate is all that is needed to evaluate the rate constant. About 20 years ago, Zusman[6] and Alexandrov[7] introduced into the theory the idea that nonequilibrium effects associated with the relaxation of solvent fluctuations could also affect the rate. In a phenomenological way, Zusman proposed a set of four partial differential equations that incorporated the relaxation of the nonequilibrium probability laws of the reaction coordinate in each diabatic state and the tunneling transitions between them. In the original model, the diabatic states are parabolic functions of the reaction coordinate, with equal curvatures for the reactant and product states. The curvature is related to the reorganization energy in such a way that equal curvatures implies that the values of the reorganization energy for the forward and backward reactions are identical. Later on, Garg *et al.*[8] presented a derivation of the Zusman equations starting from a Hamiltonian model. They use techniques of functional integrals to carry out the elimination of the bath degrees of freedom from the total density operator.

Previous analytical and numerical studies indicate that the reorganization energies for the direct and inverse reactions might indeed have different values.[9–14] It is, therefore, interesting to extend the classical Zusman–Alexandrov formulation to the case of parabolas with different curvatures. A few years ago, Tang[15] discussed such an extension. From the very beginning in his analysis, Tang made use of the so-called contact approximation. Namely, he assumed that tunneling between diabatic curves takes place strictly at their crossing points, thus neglecting any delocalization effects. Even for diabatic surfaces with equal curvatures, the fact that tunneling transitions are somewhat delocalized around the crossing point is important, especially in the inverted regime.[16,17] Delocalization leads to modifications of the rate expression with respect to the typical Marcus–Arrhenius structure. In previous work,[18] we have also found strong indications that the contact approximation is not adequate to describe strongly biased electron transfer processes.

The starting point of this paper is a set of four partial differential equations similar to those used by Tang.[15] The structure of such equations is the same as in the original Zusman model, but with parabolic potentials with different curvatures. The equations describe the dynamics of diagonal and off-diagonal matrix elements of the reduced density operator. We accept here the validity of Zusman model. Frantsuzov[19] has correctly pointed out the limitations of Zusman equations to describe electronic transfer processes in strongly polar solvents. Indeed, if the solvent polarity is too strong, the conditions under which Zusman equations are derived from a more microscopic point of view[20–23] might be

violated. This is an interesting point that we propose to address in the future. In the present work, we will concentrate on the derivation of the usual macroscopic kinetic description of electron transfer reactions from a Zusman-like model and on the determination of suitable expressions for the rate constant and the long-time populations of reactants and products. In our derivation, we will not assume the contact approximation.

The scheme of the paper is as follows: In Sec. II we set up the model and the notation. In Sec. III we derive formal expressions for the populations on the diabatic surfaces in Laplace space. This is achieved by using Green functions and projection operator techniques on the Zusman equations. An alternative method of solution of the Zusman equations has been put forward recently by Cao and Jung.[24] It is based on the spectral properties of the evolution operator for the density matrix in the Zusman approximation. As far as we know, this alternative has only been applied to diabatic parabolas of equal curvatures. The long-time limit is explicitly obtained. It is also shown that the populations satisfy integrodifferential equations with a complicated kernel. Under suitable conditions which are discussed in Sec. IV, we prove that the populations satisfy a single exponential relaxation law for all relevant time scales, characterized by the rate constant and the long-time values of the populations. In Sec. V, we present approximate analytical expressions for those two kinetic parameters. In Sec. VI we present a detailed comparison of the analytical predictions and precise numerical solution of the Zusman equations. Finally, we conclude with comments about the main findings in this work. Some of the calculations are very involved and they are presented in the Appendices.

II. THE ZUSMAN EQUATIONS FOR DIABATIC POTENTIALS WITH DIFFERENT CURVATURES

The basic elements to describe electron transfer processes are two diabatic electronic energy curves $V_j(x)$, $j=1, 2$, and a generalized one-dimensional reaction coordinate x with effective mass m. The electronic states before and after the charge transfer will be denoted as donor, $|1\rangle$, and acceptor, $|2\rangle$, respectively. The reaction coordinate represents a combination of the selected nuclear modes coupled directly to the electronic transfer system.[1] The reaction coordinate is also coupled to the rest of nuclear modes. This coupling introduces friction in the dynamics of the reaction coordinate with a phenomenological friction coefficient η. This is a well established starting point in the microscopic treatment of intramolecular electron transfer.[1,8,14] It should be noted that our $V_j(x)$ are *potential* energy curves. They should not be confused with the parabolic *free* energy curves appearing in alternative descriptions of electron transfer, as those relying on computer simulations.[10] In the overdamped limit, Zusman equations provide an appropriate description for the time evolution of the matrix elements $\rho_{jk}(x,t) := \langle j,x|\hat{\rho}(t)|x,k\rangle$ of the reduced density operator in the electron and reaction coordinate Hilbert space. Zusman equations and their validity conditions have been repeatedly derived and discussed in the literature.[8,19–23] These equations read

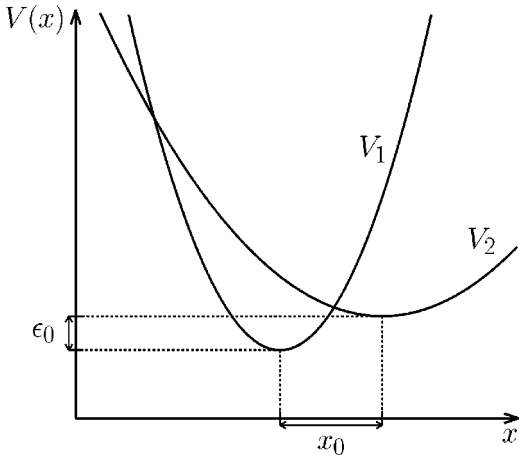

FIG. 1. Parabolic diabatic surfaces with different curvatures as a function of the reaction coordinate x. Notice that the number of crossing points depends on the value of the energy bias ϵ_0.

$$\frac{\partial}{\partial t}\rho_{11}(x,t)=\hat{\mathcal{L}}_1\rho_{11}(x,t)+i\frac{\Delta}{2\hbar}[\rho_{12}(x,t)-\rho_{21}(x,t)], \quad (1)$$

$$\frac{\partial}{\partial t}\rho_{22}(x,t)=\hat{\mathcal{L}}_2\rho_{22}(x,t)-i\frac{\Delta}{2\hbar}[\rho_{12}(x,t)-\rho_{21}(x,t)], \quad (2)$$

$$\frac{\partial}{\partial t}\rho_{12}(x,t)=\left\{\hat{\mathcal{L}}-\frac{i}{\hbar}[V_1(x)-V_2(x)]\right\}\rho_{12}(x,t) + i\frac{\Delta}{2\hbar}[\rho_{11}(x,t)-\rho_{22}(x,t)], \quad (3)$$

$$\frac{\partial}{\partial t}\rho_{21}(x,t)=\left\{\hat{\mathcal{L}}+\frac{i}{\hbar}[V_1(x)-V_2(x)]\right\}\rho_{21}(x,t) - i\frac{\Delta}{2\hbar}[\rho_{11}(x,t)-\rho_{22}(x,t)]. \quad (4)$$

Here $\hat{\mathcal{L}}_j$ are the Smoluchowski operators describing diffusion on each diabatic potential:

$$\hat{\mathcal{L}}_j=D\frac{\partial}{\partial x}\left[\frac{\partial}{\partial x}+\frac{V_j'(x)}{k_BT}\right]. \quad (5)$$

The macroscopic diffusion constant D is connected with the friction coefficient η, which is assumed to be identical in both diabatic states, and the temperature T by the Einstein relation $D=k_BT/\eta$. The operator $\hat{\mathcal{L}}=(\hat{\mathcal{L}}_1+\hat{\mathcal{L}}_2)/2$ describes diffusion on the average potential $[V_1(x)+V_2(x)]/2$. Finally, Δ denotes the electronic coupling matrix element, and it characterizes the degree of overlap of the donor and acceptor wave functions. Here, we will take Δ to be independent of the nuclear coordinates (Condon approximation).

In this work, we will assume parabolic diabatic curves of the form

$$V_j(x)=\frac{m\omega_j^2}{2}(x-x_0\delta_{j,2})^2-\epsilon_0\delta_{j,2}, \quad (6)$$

where x_0 and ϵ_0 are the horizontal and vertical shifts, respectively, between the minima of the parabolas (cf. Fig. 1). The frequencies ω_j characterize their curvatures, and they are

related to the reorganization energies λ_j by the expression $\lambda_j = m\omega_j^2 x_0^2/2$. Therefore, the fact that the curvatures are different implies that these reorganization energies for the forward and backward reactions are also different. To avoid confusion, we want to emphasize that the curvatures of our diabatic potential energies, ω_j, can be different. If one describes electron transfer processes in terms of free energy profiles, then, as pointed out by Tachiya,[25] the two free energy curves are not independent, and they cannot be strictly parabolic when the curvatures at their minima are different. Obviously, our *potential* energies, not being *free* energies, are not tied up by such a restriction. The difference in curvatures also yields a difference in the phenomenological relaxation times corresponding to each diabatic curve,

$$\tau_j = \frac{\eta}{m\omega_j^2} = \frac{k_B T}{m\omega_j^2 D}. \tag{7}$$

Notice that these relaxation times are related to the reorganization energies by $\tau_1/\tau_2 = \lambda_2/\lambda_1$. For later convenience, we will also introduce the relaxation time of the overdamped oscillator on the averaged potential $[V_1(x)+V_2(x)]/2$,

$$\tau = \frac{2k_B T}{mD(\omega_1^2+\omega_2^2)}. \tag{8}$$

From the above expressions, it follows that $2/\tau = 1/\tau_1 + 1/\tau_2$.

Electron tunneling is most effective near the crossing points of the diabatic curves, which are given by

$$x_j^* = \frac{x_0}{\lambda_2-\lambda_1}\left[\lambda_2 + (-1)^j\sqrt{\left(1-\frac{\epsilon_0}{\epsilon_c}\right)\lambda_1\lambda_2}\right], \tag{9}$$

where $\epsilon_c = \lambda_1\lambda_2/(\lambda_1-\lambda_2)$. Depending on the relative values of ϵ_0 and ϵ_c there can be two, one, or no crossing points.

III. FORMAL SOLUTION OF THE ZUSMAN EQUATIONS

In this section we obtain some exact, though formal, analytical results for the time evolution of the populations $P_j(t)$. They are obtained by integrating the corresponding probability densities over configuration space, i.e., $P_j(t) = \int_{-\infty}^{\infty} dx\, \rho_{jj}(x,t)$. The first step is to reduce the four Zusman equations to just two integral equations for the diagonal elements $\rho_{jj}(x,t)$. This is achieved by first replacing $\rho_{12}(x,t)$ and $\rho_{21}(x,t)$ in Eqs. (1) and (2) by the result of formally solving the two off-diagonal equations (3) and (4). This yields

$$\begin{aligned}\frac{\partial}{\partial t}\rho_{jj}(x,t) = {} & \frac{(-1)^j\Delta}{\hbar}\int_{-\infty}^{\infty} dx_1\ \mathrm{Im}[G_{od}(x,t|x_1)\rho_{12}(x_1,0)] \\ & + \frac{(-1)^j\Delta^2}{2\hbar^2}\int_0^t dt_1 \int_{-\infty}^{\infty} dx_1 \\ & \times \mathrm{Re}[G_{od}(x,t-t_1|x_1)] \\ & \times [\rho_{11}(x_1,t_1)-\rho_{22}(x_1,t_1)] + \hat{\mathcal{L}}_j\,\rho_{jj}(x,t),\end{aligned} \tag{10}$$

where $G_{od}(x,t|x')$, the off-diagonal Green function, is the solution of the partial differential equation

$$\frac{\partial}{\partial t}G_{od}(x,t|x') = \left\{\hat{\mathcal{L}} - \frac{i}{\hbar}[V_1(x)-V_2(x)]\right\}G_{od}(x,t|x'), \tag{11}$$

with initial condition

$$G_{od}(x,0|x') = \delta(x-x'), \tag{12}$$

and boundary conditions

$$\lim_{x\to\pm\infty} G_{od}(x,t|x') = 0. \tag{13}$$

An evaluation of this Green function for the harmonic potentials with different curvatures can be found in Appendix A 1. From now on, we shall assume that $\rho_{12}(x,0)=0$, so that the first term on the right-hand side of expression (10) will not be present. This initial condition describes the usual situation in which the electronic coherences between donor and acceptor states are initially neglected.

Next, formal solution of Eq. (10) in terms of the diagonal Green functions $G_d^{(j)}(x,t|x')$ leads to

$$\begin{aligned}\rho_{jj}(x,t) = {} & (-1)^j\int_0^t dt_1\int_{-\infty}^{\infty} dx_1\, a_j(x,t-t_1|x_1) \\ & \times[\rho_{11}(x_1,t_1)-\rho_{22}(x_1,t_1)] \\ & + \int_{-\infty}^{\infty} dx_1\, G_d^{(j)}(x,t|x_1)\rho_{jj}(x_1,0).\end{aligned} \tag{14}$$

The propagators $a_j(x,t|x')$ in Eq. (14) are given in terms of the Green functions by

$$\begin{aligned}a_j(x,t|x') = {} & \frac{\Delta^2}{2\hbar^2}\int_0^t dt' \int_{-\infty}^{\infty} dx''\, G_d^{(j)}(x,t \\ & - t'|x'')\ \mathrm{Re}[G_{od}(x'',t'|x')].\end{aligned} \tag{15}$$

The diagonal Green functions describe the diffusive motion on the diabatic curves $V_j(x)$. They are the solution of the partial differential equations

$$\frac{\partial}{\partial t}G_d^{(j)}(x,t|x') = \hat{\mathcal{L}}_j G_d^{(j)}(x,t|x'), \tag{16}$$

with the same type of initial and boundary conditions as $G_{od}(x,t|x')$. Explicit expressions for $G_d^{(j)}(x,t|x')$ can be found in Appendix A 2.

Typically, a reaction starts from a situation where the solvent is thermally equilibrated. Thus, we will restrict our study to initial conditions for the diagonal terms of the form $\rho_{jj}(x,0) = g_j(x)P_j(0)$, where

$$g_j(x) = \frac{\exp[-V_j(x)/k_B T]}{\int_{-\infty}^{\infty} dx'\,\exp[-V_j(x')/k_B T]} \tag{17}$$

are the equilibrium distributions on each of the diabatic curves, and $P_j(0)$ are the initial conditions for the populations. Obviously, with these initial conditions, the second term on the right-hand side of expression (14) reduces to $g_j(x)P_j(0)$.

For later convenience, we will rewrite Eq. (14) in matrix notation by introducing the one-column vector $\varrho(x,t)$ with components $\varrho_j(x,t)=\rho_{jj}(x,t)$, and the 2×2 matrices $\boldsymbol{U}$, $\boldsymbol{A}(x,t|x')$, and $\boldsymbol{g}(x)$ with matrix elements $U_{jk}=(-1)^{j+k}$, $A_{jk}(x,t|x')=a_j(x,t|x')\delta_{j,k}$, and $g_{jk}(x)=g_j(x)\delta_{j,k}$, respectively. The solution of Eq. (14) is best sought by using the Laplace transform $\tilde{f}(s)=\int_0^\infty dt\, f(t)\exp(-st)$. Thus, one finds

$$\tilde{\varrho}(x,s)=s^{-1}\boldsymbol{g}(x)\boldsymbol{P}(0)-\int_{-\infty}^{\infty}dx_1\,\tilde{\boldsymbol{A}}(x,s|x_1)\boldsymbol{U}\tilde{\varrho}(x_1,s). \quad (18)$$

We will use standard projection operator techniques to get an expression for the Laplace transform of the populations $\tilde{\boldsymbol{P}}(s)$. We define the projection operators Π and Q as

$$\Pi\boldsymbol{F}(x)=\boldsymbol{F}_{\|}(x)=\boldsymbol{g}(x)\int_{-\infty}^{\infty}dx'\boldsymbol{F}(x'), \quad (19)$$

$$Q\boldsymbol{F}(x)=\boldsymbol{F}_{\perp}(x)=\boldsymbol{F}(x)-\boldsymbol{F}_{\|}(x), \quad (20)$$

$\boldsymbol{F}(x)$ being an arbitrary one-column vector or 2×2 matrix depending on x. By acting with Π on Eq. (18) and integrating over x, one obtains after some simplifications

$$\boldsymbol{P}(0)=\left[s\boldsymbol{I}+\int_{-\infty}^{\infty}dx_1\,\tilde{K}(x_1,s)\boldsymbol{U}\boldsymbol{g}(x_1)\right]\tilde{\boldsymbol{P}}(s)+\int_{-\infty}^{\infty}dx_1\,\tilde{K}(x_1,s)\boldsymbol{U}\tilde{\varrho}_{\perp}(x_1,s), \quad (21)$$

where $\boldsymbol{I}$ is the 2×2 unit matrix and

$$\tilde{K}(x,s)=\frac{\Delta^2}{2\hbar^2}\int_{-\infty}^{\infty}dx'\ \mathrm{Re}[\tilde{G}_{od}(x',s|x)]. \quad (22)$$

Using Eq. (A16) in Eq. (22), we obtain

$$\tilde{K}(x,s)=\frac{\Delta^2}{2\hbar^2}\int_0^\infty dt\ \mathrm{Re}\{\exp[-st-c(t,x)]\}, \quad (23)$$

with $c(t,x)$ given by Eq. (A11). The action of Q on Eq. (18) leads to

$$\tilde{\varrho}_{\perp}(x,s)=-\int_{-\infty}^{\infty}dx_1\,\tilde{\boldsymbol{A}}_{\perp}(x,s|x_1)\boldsymbol{U}[\boldsymbol{g}(x_1)\tilde{\boldsymbol{P}}(s)+\tilde{\varrho}_{\perp}(x_1,s)], \quad (24)$$

where

$$\tilde{\boldsymbol{A}}_{\perp}(x,s|x')=\frac{\Delta^2}{2\hbar^2}\boldsymbol{g}(x)\int_{-\infty}^{\infty}dx''\tilde{\boldsymbol{J}}(x,s|x'')\times\mathrm{Re}[\tilde{G}_{od}(x'',s|x')], \quad (25)$$

with $\tilde{\boldsymbol{J}}(x,s|x')$ being the 2×2 diagonal matrix with matrix elements

$$\tilde{J}_{jk}(x,s|x')=\delta_{j,k}\{[g_j(x)]^{-1}\tilde{G}_d^{(j)}(x,s|x')-s^{-1}\}. \quad (26)$$

A formal solution for $\tilde{\varrho}_{\perp}(x,s)$ is obtained by solving iteratively the integral equation (24). Substitution of the result in Eq. (21) leads to

$$\boldsymbol{P}(0)=[s\,\boldsymbol{I}+\boldsymbol{U}\tilde{\boldsymbol{k}}(s)]\tilde{\boldsymbol{P}}(s), \quad (27)$$

where $\tilde{\boldsymbol{k}}(s)$ is the diagonal matrix obtained by summing the series

$$\tilde{\boldsymbol{k}}(s)=\sum_{n=1}^{\infty}\tilde{\boldsymbol{k}}^{(n)}(s). \quad (28)$$

The terms of the series $\tilde{\boldsymbol{k}}^{(n)}(s)$ are given by

$$\tilde{\boldsymbol{k}}^{(1)}(s)=\int_{-\infty}^{\infty}dx_1\,\tilde{K}(x_1,s)\boldsymbol{g}(x_1) \quad (29)$$

and

$$\tilde{\boldsymbol{k}}^{(n)}(s)=(-1)^{n-1}\int_{-\infty}^{\infty}dx_1\cdots\int_{-\infty}^{\infty}dx_n\,\tilde{K}(x_1,s)\times\prod_{j=2}^{n}\mathrm{Tr}[\tilde{\boldsymbol{A}}_{\perp}(x_{j-1},s|x_j)]\boldsymbol{g}(x_n) \quad (30)$$

for $n\geqslant2$.

According to Eq. (27), the Laplace transform of the populations can be expressed in terms of the diagonal matrix $\tilde{\boldsymbol{k}}(s)$ as

$$\tilde{P}_j(s)=\frac{P_j(0)+s^{-1}[\delta_{j,1}\tilde{k}_{22}(s)+\delta_{j,2}\tilde{k}_{11}(s)]}{s+\tilde{k}_{11}(s)+\tilde{k}_{22}(s)}. \quad (31)$$

After carrying out the inverse Laplace transform of the above expression, one obtains the time evolution of the populations, $P_j(t)$. It follows from expression (31) that the long-time limit of the populations is given by

$$P_j(\infty)\coloneqq\lim_{t\to+\infty}P_j(t)=\lim_{s\to0+}s\tilde{P}_j(s)=\frac{\delta_{j,1}\tilde{k}_{22}(0)+\delta_{j,2}\tilde{k}_{11}(0)}{\tilde{k}_{11}(0)+\tilde{k}_{22}(0)}. \quad (32)$$

Notice that these values are independent of the initial conditions $P_j(0)$.

Finally, rearranging Eq. (27) and carrying out the inverse Laplace transform, we find that the populations $P_j(t)$ satisfy the set of generalized master equations

$$\begin{aligned}\frac{d}{dt}P_1(t)&=-\int_0^t dt'\,[k_{11}(t-t')P_1(t')-k_{22}(t-t')P_2(t')],\\ \frac{d}{dt}P_2(t)&=-\int_0^t dt'\,[k_{22}(t-t')P_2(t')-k_{11}(t-t')P_1(t')],\end{aligned} \quad (33)$$

where $k_{jj}(t)$ is the inverse Laplace transform of $\tilde{k}_{jj}(s)$. From the above set of equations, it follows immediately the conservation of probability, i.e., $P_1(t)+P_2(t)=1$. Thus, the set (33) reduces to a single integrodifferential equation for, say, the population $P_1(t)$. This equation can be conveniently written as

$$\frac{d}{dt}P_1(t)=-\int_0^t dt'\,[k_{11}(t')+k_{22}(t')]P_1(t-t')+\int_0^t dt'\,k_{22}(t'). \quad (34)$$

Then, after solution of Eq. (34), the evolution of $P_2(t)$ follows immediately.

Up to now, the formal results that we have obtained are exact. We have only assumed the convergence of the series (28) and a specific family of initial conditions for the densi-

ties $\rho_{jk}(x,t)$. The result (33) is important. The populations on the donor and acceptor diabatic curves satisfy first order integrodifferential equations with a convolution structure. The convolution kernels, $k_{jj}(t)$, are rather complicated. The next important task is to analyze under which conditions can the solutions of Eq. (33) be properly approximated by a single exponential time evolution.

IV. VALIDITY CONDITIONS FOR THE RATE REGIME

In kinetics, the time evolution of the populations on the donor, $P_1(t)$, and acceptor, $P_2(t)$, diabatic curves is usually given by

$$P_j(t)=P_j(\infty)+[P_j(0)-P_j(\infty)]e^{-\Gamma t}, \tag{35}$$

where Γ is the total rate constant. In this section we analyze the conditions under which this rate description of the time evolution of the populations can be obtained from the Zusman equations. The starting point is the integrodifferential equation (34). In this equation one can distinguish two different clear-cut time scales. The first one, τ_a, is associated with the relaxation time of the kernels $k_{jj}(t)$. As all the time dependence of $k_{jj}(t)$ is through the diagonal and off-diagonal Green functions, τ_a depends mainly on the relaxation times of these Green functions. The second one is given by $\tau_b=[\tilde{k}_{11}(0)+\tilde{k}_{22}(0)]^{-1}$ and, as we will see below, it is associated with the relaxation time of the populations. In general, τ_b depends on the relaxation times of the Green functions and also on the characteristic tunneling time scale $\hbar/\Delta$. In the next section, we will obtain approximate expressions for τ_b^{-1}.

In order to study the validity conditions for the rate regime, it is convenient to express Eq. (34) in dimensionless form as

$$\frac{d}{dY}P_1(Y;\zeta)=-\int_0^{Y/\zeta}dy'\,[\kappa_{11}(y')+\kappa_{22}(y')]P_1(Y-\zeta y';\zeta)+\int_0^{Y/\zeta}dy'\,\kappa_{22}(y'). \tag{36}$$

Here we have introduced the dimensionless quantities $Y=t/\tau_b$, $y'=t'/\tau_a$, $\zeta=\tau_a/\tau_b$, and $\kappa_{jj}(y')=\tau_a\tau_b k_{jj}(\tau_a y')$, and we have indicated explicitly the dependence of $P_1(Y;\zeta)$ on the parameter ζ. Notice that the dimensionless integration variable y' has been chosen so that the contributions of the integrand for values of y' much larger than unity can be safely neglected.

Let us assume that we are in a regime in which $\tau_a \ll \tau_b$. To find the leading-order approximation to the solution of Eq. (36) as $\zeta\to 0+$, i.e., $P_1(Y;0)=\lim_{\zeta\to 0+}P_1(Y;\zeta)$, we take the limit $\zeta\to 0+$ in Eq. (36) while keeping $Y\neq 0$ fixed. The result is

$$\frac{d}{dY}P_1(Y;0)=-\int_0^{\infty}dy'\,[\kappa_{11}(y')+\kappa_{22}(y')]P_1(Y;0)+\int_0^{\infty}dy'\,\kappa_{22}(y')=-P_1(Y;0)+P_1(\infty), \tag{37}$$

where we have taken into account that the values of the integrand for y' much larger than unity are negligible. The solution of Eq. (37) is $P_1(Y;0)=Ce^{-Y}+P_1(\infty)$, C being an unknown constant of integration. This constant is determined by making use of the initial condition, i.e., $\lim_{Y\to 0+}P_1(Y;0)=C+P_1(\infty)=P_1(0)$. Therefore, after going back to the original variable t, we find that the leading-order approximation to the solution of Eq. (36) as $\zeta\to 0+$ is given by Eq. (35) with $j=1$ and $\Gamma=\tau_b^{-1}$. From the conservation of probability, it follows immediately that, in this limit, the population $P_2(t)$ is also of the form (35).

In conclusion, we have proved that, when $\tau_a \ll \tau_b$, the values of the populations obtained from the Zusman equations can be properly approximated by the rate expression (35) with total rate

$$\Gamma=\tilde{k}_{11}(0)+\tilde{k}_{22}(0). \tag{38}$$

Notice that, when $\tau_a \ll \tau_b$, Eq. (35) describes properly the relaxation of the populations for all the relevant time scales associated with $P_j(t)$, even for short times. When the condition $\tau_a \ll \tau_b$ is violated, then the discrepancies between the predictions of Eq. (35) and those of the Zusman equations might be relevant at all times, as we will see later, when we compare with numerical solution of Zusman equation (see Sec. VI).

V. ANALYTICAL EXPRESSIONS FOR THE LONG-TIME POPULATIONS AND THE TOTAL RATE CONSTANT

From now on, we will assume that a rate description of the time evolution of the populations is appropriate. In that case, the parameters $P_j(\infty)$ and Γ can be expressed in terms of the diagonal matrix $\tilde{\boldsymbol{k}}(0)$, according to Eqs. (32) and (38). The evaluation of this matrix entails the summation of the series (28). In order to do so, one has to resort to approximations. The nature of the approximations is dictated by the relative values of the tunneling frequency and the characteristic frequencies of the solvent dynamics.

A. The nonadiabatic limit

If the characteristic tunneling frequency $\Delta/\hbar$ is very small relative to the relaxation frequencies associated with the Green functions, then tunneling becomes the limiting step mechanism of the rate process. In this nonadiabatic regime, the matrix elements of $\tilde{\boldsymbol{k}}(0)$ can be approximated as

$$\tilde{k}_{jj}(0)\approx k_{\mathrm{NA}}^{(j)}:=\Delta^2\lim_{\Delta\to 0}\frac{\tilde{k}_{jj}(0)}{\Delta^2}=\tilde{k}_{jj}^{(1)}(0). \tag{39}$$

After inserting the expressions (17) and (23), with $s=0$, into Eq. (29) and integrating over x_1, we find

$$k_{\mathrm{NA}}^{(j)}=\frac{\Delta^2\Lambda_j^{1/2}}{\hbar^2}\int_0^{\infty}dt\ \mathrm{Re}\{N_j(t)\exp[R_j(t)]\}, \tag{40}$$

where

$$N_j(t)=\frac{\alpha^{1/2}\exp[(1-\alpha)t/(2\tau)]}{\{(\alpha+1)[2\Lambda_j+(\alpha-1)/2]+(\alpha-1)[2\Lambda_j-(\alpha+1)/2]\exp[-2\alpha t/\tau]\}^{1/2}}, \tag{41}$$

$$R_j(t)=i\left[\frac{\lambda_1\lambda_2(\Lambda_1-\Lambda_2+i\chi)}{\hbar(\lambda_1+\lambda_2)\alpha^2}-\frac{\epsilon_0}{\hbar}\right]t+\frac{4\tau\lambda_1^2\lambda_2^2}{\hbar\lambda_j(\lambda_1+\lambda_2)^2\alpha^3}$$
$$\times\left\{\frac{[i(2\Lambda_j+1)(-1)^{j-1}+\chi]\alpha\sinh(\alpha t/\tau)}{4\Lambda_j\alpha\cosh(\alpha t/\tau)+[4\Lambda_j+\alpha^2-1]\sinh(\alpha t/\tau)}+\frac{2\Lambda_j[2i(-1)^{j-1}+\chi][\cosh(\alpha t/\tau)-1]}{4\Lambda_j\alpha\cosh(\alpha t/\tau)+[4\Lambda_j+\alpha^2-1]\sinh(\alpha t/\tau)}\right\}, \tag{42}$$

and the dimensionless parameters Λ_j, χ, and α are defined in Eqs. (A12)–(A14). The remaining time integral in Eq. (40) can be calculated by a numerical quadrature. The expressions for the long-time populations and the rate constant in the nonadiabatic limit, $P_j^{(\mathrm{NA})}(\infty)$ and Γ_{NA}, are obtained by replacing $\tilde{k}_{jj}(0)$ with $k_{\mathrm{NA}}^{(j)}$ in Eqs. (32) and (38). To the best of our knowledge, Eqs. (40)–(42) have never been derived previously in the literature. These expressions for the nonadiabatic parameters are one of the main results in this paper. They constitute a generalization of the typical golden rule rate expressions to the case of diabatic parabolas with different curvatures. Notice that we are not assuming that the tunneling transitions are exactly localized at the crossing points of the parabolas as it is assumed in the so-called contact approximation.[15,18] Actually, our expressions reflect the delocalization induced by the solvent dynamics. This delocalization might be important. As we have previously shown,[18] detailed comparison of the results obtained with the rate formulas, with and without the contact approximation, and the results of the numerical solution of the Zusman equations indicates that the rate expressions with the contact approximation become invalid for large values of the energy bias, ϵ_0.

For the case of equal curvatures, $\lambda_1=\lambda_2=\lambda$, Eq. (40) reduces to the known result[21]

$$k_{\mathrm{NA}}^{(j)}=\frac{\Delta^2}{2\hbar^2}\int_0^\infty dt\ \exp\left[\frac{2\lambda k_BT\tau^2}{\hbar^2}\left(1-e^{-t/\tau}-\frac{t}{\tau}\right)\right]$$
$$\times\cos\left[\frac{\lambda\tau}{\hbar}(1-e^{-t/\tau})+\frac{(-1)^j\epsilon_0}{\hbar}t\right]. \tag{43}$$

In this case, the time integral can be evaluated explicitly in terms of the complete $[\Gamma(x)]$ and incomplete $[\Gamma(x,y)]$ Gamma functions[26] as

$$k_{\mathrm{NA}}^{(j)}=\frac{\Delta^2\tau}{2\hbar^2}\,\mathrm{Re}\{e^b b^{-a_j}[\Gamma(a_j)-\Gamma(a_j,b)]\}, \tag{44}$$

where we have introduced the dimensionless parameters $a_j=\tau[2\lambda k_BT\tau/\hbar-(-1)^j i\epsilon_0]/\hbar$ and $b=\tau\lambda[2k_BT\tau/\hbar+i]/\hbar$. By the relation $\gamma(a,x):=\Gamma(a)-\Gamma(a,x)=a^{-1}x^a e^{-x}M(1,1+a,x)$,[27] where $M(a,b,c)$ is the Kummer's function, our Eq. (44) is equivalent to Eq. (3.13) in Ref. 19.

It should be noticed that, as Frantsuzov[19] has pointed out, Eq. (43) can lead to nonphysical predictions, such as violation of the detailed balance and negative values for the rates in strongly polar solvents with large reorganization energies. As we discuss in Sec. VI, in the case of different reorganization energies and $\epsilon_0>\epsilon_c$, we have also observed deviations between the values of the long-time populations predicted by Eqs. (32) and (40)–(42) and those expected from statistical thermodynamical considerations in the semiclassical limit. These anomalous results, which are intrinsic to the Zusman equations, can be used as a numerical criterion in order to test the validity of the Zusman description of ET reactions.

The expressions for the nonadiabatic rate constants (40)–(42) [or Eq. (43) in the case of equal curvatures] simplify considerably if one makes use of the contact approximation. Within this approximation, one assumes that the electronic transitions take place precisely at the crossing points, so that, the function $\tilde{K}(x,0)$ in Eq. (29) can be approximated by

$$\tilde{K}(x,0)\simeq\frac{\pi\Delta^2}{2\hbar}\,\delta[V_1(x)-V_2(x)]. \tag{45}$$

Then, the nonadiabatic rate constant, for $\epsilon_0<\epsilon_c$, can be expressed as[15,18]

$$k_{\mathrm{NA}}^{(1)}=\frac{\Delta^2}{4\hbar}\sqrt{\frac{\pi}{k_BT\lambda_2(1-\epsilon_0/\epsilon_c)}}\left\{\exp\left[-\frac{(\lambda_2-\epsilon_0)^2}{4\lambda_+(\epsilon_0)k_BT}\right]\right.$$
$$\left.+\exp\left[-\frac{(\lambda_2-\epsilon_0)^2}{4\lambda_-(\epsilon_0)k_BT}\right]\right\}, \tag{46}$$

$$k_{\mathrm{NA}}^{(2)}=\sqrt{\frac{\lambda_2}{\lambda_1}}\exp\left(-\frac{\epsilon_0}{k_BT}\right)k_{\mathrm{NA}}^{(1)}, \tag{47}$$

where we have defined the auxiliary, bias-dependent quantities

$$\lambda_\pm(\epsilon_0)=\frac{[\lambda_2\pm\sqrt{(1-\epsilon_0/\epsilon_c)\lambda_1\lambda_2}]^2}{4\lambda_1}. \tag{48}$$

This contact approximation plays an essential role in Tang's analysis of the Zusman equations.[15] In the case of equal curvatures, the nonadiabatic rate constants in Eqs. (46) and (47) reduce to the celebrated Marcus–Levich–Dogonadze rate[3,5] and, therefore, they can be considered as its natural generalization to the case of different curvatures.

B. The consecutive step approximation

In order to go beyond the nonadiabatic limit, we need to evaluate the series in Eq. (28). We will do this by extending the *consecutive step approximation*[20,21] to the case of differ-

ent reorganization energies for the forward and backward reactions. In this approximation, the terms of the series are simplified after disentangling the dynamical effects associated with diffusion from those relying on tunneling. We will assume that the function $\tilde{\boldsymbol{J}}(x,0|x'')$ in Eq. (26) varies in x'' with a characteristic scale much larger than the width of the interval around x' where $\tilde{G}_{od}(x'',0|x')$ differs appreciably from zero. Then, according to Eqs. (22) and (25), one can approximate

$$\tilde{\boldsymbol{A}}_{\perp}(x,0|x') \approx \boldsymbol{g}(x)\tilde{\boldsymbol{J}}(x,0|x')\tilde{K}(x',0). \tag{49}$$

With this simplified expression for $\tilde{\boldsymbol{A}}_{\perp}(x,0|x')$, the exact expression in Eq. (30) for the terms $\tilde{\boldsymbol{k}}^{(n)}(0)$ in the series expansion can be approximated by

$$\tilde{\boldsymbol{k}}^{(n)}(0) \approx (-1)^{n-1} \int_{-\infty}^{\infty} dx_1 \ldots \int_{-\infty}^{\infty} dx_n \tilde{K}(x_n,0)\boldsymbol{g}(x_n) \times \prod_{j=2}^{n} \mathrm{Tr}[\tilde{K}(x_{j-1},0)\boldsymbol{g}(x_{j-1})\tilde{\boldsymbol{J}}(x_{j-1},0|x_j)] \tag{50}$$

for $n \geqslant 2$. Henceforth, we will assume that there are two crossing points, i.e., $\epsilon_0 < \epsilon_c$. Then, as it can be checked by numerical integration of Eq. (23) with $s=0$, the function $\tilde{K}(x,0)$ shows peaks of similar heights and widths centered at the crossing points, at least when they are well separated. Assuming that the characteristic scale of variation of the functions $\tilde{\boldsymbol{J}}(x,0|x')$ and $\boldsymbol{g}(x)$ are also much larger than the widths of those peaks, we finally obtain that, for $n \geqslant 2$, the matrices $\tilde{\boldsymbol{k}}^{(n)}(0)$ can be well approximated by

$$\tilde{\boldsymbol{k}}^{(n)}(0) \approx \nu^{(n)} \tilde{\boldsymbol{k}}^{(1)}(0), \tag{51}$$

where

$$\nu^{(n)} = (-1)^{n-1} \sum_{j_1=1}^{2} \cdots \sum_{j_n=1}^{2} r_{j_1} \cdots r_{j_n} \times \prod_{l=2}^{n} \mathrm{Tr}[\tilde{\boldsymbol{k}}^{(1)}(0)\tilde{\boldsymbol{J}}(x_{j_{l-1}}^{*},0|x_{j_l}^{*})]. \tag{52}$$

In the above expression, x_j^* represents the coordinate of the jth crossing point given by Eq. (9), and the coefficients

$$r_j = \frac{g_1(x_j^*)}{g_1(x_1^*)+g_1(x_2^*)} = \frac{g_2(x_j^*)}{g_2(x_1^*)+g_2(x_2^*)} \tag{53}$$

denote the equilibrium weights of the two crossing points contributions. Then, according to Eq. (28), we find that

$$\tilde{\boldsymbol{k}}(0) \approx \nu\, \tilde{\boldsymbol{k}}^{(1)}(0), \tag{54}$$

where ν is the result of summing up the series

$$\nu = \sum_{n=1}^{\infty} \nu^{(n)}, \tag{55}$$

with $\nu^{(1)}=1$. In Appendix B we carry out the summation of this series explicitly [cf. Eq. (B7)]. The traces appearing in Eq. (B7) (the coefficients $\Xi_{l,m}$) can be expressed in terms of the nonadiabatic rate constants, $k_{\mathrm{NA}}^{(j)}$, as

$$\mathrm{Tr}[\tilde{\boldsymbol{k}}^{(1)}(0)\tilde{\boldsymbol{J}}(x_l^*,0|x_m^*)] = \sum_{n=1}^{2} \frac{k_{\mathrm{NA}}^{(n)}}{k_{D_{lm}}^{(n)}}. \tag{56}$$

Here, according to Eqs. (26) and (A18), we have defined the coefficients $k_{D_{lm}}^{(j)}$ as

$$\frac{1}{k_{D_{lm}}^{(j)}} := \lim_{s\to 0+} \tilde{J}_{jj}(x_l^*,s|x_m^*) = \tau_j \int_0^{\infty} dz \left\{ \frac{\exp\left[\frac{\lambda_j}{2k_BT}\left(\frac{(y_l+y_m-2\delta_{j,2})^2}{e^z+1} - \frac{(y_l-y_m)^2}{e^z-1}\right)\right]}{(1-e^{-2z})^{1/2}} - 1 \right\}, \tag{57}$$

where we have expressed the time integral in dimensionless units, and we have introduced the dimensionless coordinates of the crossing points $y_l = x_l^*/x_0$. The coefficients $k_{D_{lm}}^{(j)}$ arise from the diffusional dynamics along the diabatic surfaces. The diagonal terms $k_{D_{ll}}^{(j)}$ can be expressed through the generalized hypergeometric functions,[26] ${}_2F_2(a,b;c,d;z)$, as[21,18]

$$\frac{1}{k_{D_{ll}}^{(j)}} = \tau_j \left[\ln 2 + \frac{2E_{a_l}^{(j)}}{k_BT}\, {}_2F_2\left(1,1;\frac{3}{2},2;\frac{E_{a_l}^{(j)}}{k_BT}\right)\right], \tag{58}$$

where $E_{a_l}^{(j)}$ are the activation energies measured from the bottom of the diabatic potential $V_j(x)$ to the crossing point x_l^*, i.e., $E_{a_l}^{(j)} = V_j(x_l^*) + \epsilon_0\, \delta_{j,2}$.

Finally, taking into account Eqs. (54), (56), and (B7), we can conclude that, in the consecutive step approximation (CSA), the matrix elements of $\tilde{\boldsymbol{k}}(0)$ can be approximated as

$$\tilde{k}_{jj}(0) \approx k_{\mathrm{CSA}}^{(j)} := \frac{1 + r_1 r_2 \sum_{n=1}^{2}\sum_{l=1}^{2}\sum_{m=1}^{2} (-1)^{l+m} \frac{k_{\mathrm{NA}}^{(n)}}{k_{D_{lm}}^{(n)}}}{\prod_{l=1}^{2}\left[1 + r_l \sum_{n=1}^{2} \frac{k_{\mathrm{NA}}^{(n)}}{k_{D_{ll}}^{(n)}}\right] - r_1 r_2 \left[\sum_{n=1}^{2} \frac{k_{\mathrm{NA}}^{(n)}}{k_{D_{12}}^{(n)}}\right]^2} k_{\mathrm{NA}}^{(j)}. \tag{59}$$

The expressions for the long-time populations and the rate constant in the consecutive step approximation, $P_j^{(\mathrm{CSA})}(\infty)$ and Γ_{CSA}, are obtained by replacing $\tilde{k}_{jj}(0)$ with $k_{\mathrm{CSA}}^{(j)}$ in Eqs. (32) and (38). Notice that the equilibrium populations in the consecutive step approximation coincide with those obtained

within the nonadiabatic limit, namely, $P_j^{(\mathrm{CSA})}(\infty) = P_j^{(\mathrm{NA})}(\infty)$. This can be easily seen after substitution of Eq. (59) into Eq. (32).

As we have previously analyzed,[18] if the crossing point x_2^* is much higher in energy than x_1^*, then one can replace in Eq. (59) $r_1 \Rightarrow 1$ and $r_2 \Rightarrow 0$. In this case, expression (59) simplifies considerably to

$$k_{\mathrm{CSA}}^{(j)} \approx \frac{k_{\mathrm{NA}}^{(j)}}{1 + k_{\mathrm{NA}}^{(1)}/k_{D_{11}}^{(1)} + k_{\mathrm{NA}}^{(2)}/k_{D_{11}}^{(2)}}. \tag{60}$$

The above formula has the same structure as the one used in the literature for equal curvatures.[20,21] Equation (59) and its simplified version, Eq. (60), describe in a unified way the different rate regimes, ranging from nonadiabatic to solvent controlled adiabatic reactions, depending upon the relative values of the system parameters characterizing tunneling and diffusion.

The derivation of Eq. (59) is one of the main results of this paper, and as far as we know, it has never been obtained before. A few years ago, Tang[15] arrived to an expression somewhat similar to Eq. (59). A detailed comparison of our work and that of Tang reveals, nonetheless, some important differences. First, Tang neglects the off-diagonal diffusion terms, $k_{D_{12}}^{(j)}$, present in our Eq. (59). Second, the nonadiabatic rate constants appearing in Tang's expression are the ones obtained within the contact approximation [cf. Eqs. (46)–(48)].

VI. COMPARISON WITH NUMERICAL RESULTS AND DISCUSSION

In this section we shall compare our analytical results with those provided by numerical integration of the Zusman equations. The latter has been carried out using the standard numerical algorithm group routine D03PCF on a LINUX PC with an Intel 800 MHz processor. In the numerical procedure, artificial absorbing boundary conditions have been properly superimposed far away from the reaction region, in order to model the natural boundary conditions, $\rho_{ij}(x,t) \to 0$ at $x \to \pm\infty$. Such a modeling did not affect the quality of the numerics, which was controlled by the numerical conservation of the total probability $P_1(t) + P_2(t) = 1$ on the whole time scale. Namely, the deviation of the total probability from unity did not exceed 3×10^{-7} for the mesh of 1500 space points and the single time step accuracy parameter of 10^{-7}. We have adjusted both the number of mesh points and the time accuracy in order to achieve convergence of the results within the width of the plotted curves. Depending upon the values of the parameters, the calculation of a relaxation curve involving 100 time points took from about several seconds to about half an hour. The long-time population, $P_1(\infty)$, and the rate constant, Γ, have been extracted from the numerical $P_1(t)$ making use of a nonlinear, single-exponential fitting procedure in GNUPLOT.

The following set of parameter values is kept fixed in the calculations: $\lambda_1 = 800\ \mathrm{cm}^{-1}$, $\lambda_2 = 200\ \mathrm{cm}^{-1}$, $T = 300$ K. The other parameters, ϵ_0, Δ, and τ, have been varied. Strongly different values for the reorganization energies λ_1 and λ_2 have been chosen on purpose, in order to demonstrate the quality of our analytical results. In realistic situations, the difference between the reorganization energies may not be so dramatically large. For example, it was found in Ref. 10 that the reaction of primary charge separation in the bacterial photosynthetic center immersed in a nonpolar lipid membrane occurs with $\lambda_1 \approx 1.45$ kcal/mol$\approx 507.22\ \mathrm{cm}^{-1}$, $\lambda_2 \approx 1.55$ kcal/mol$\approx 542.20\ \mathrm{cm}^{-1}$. In such a case, we expect our approximate results to work even better for a similar set of the remaining parameters.

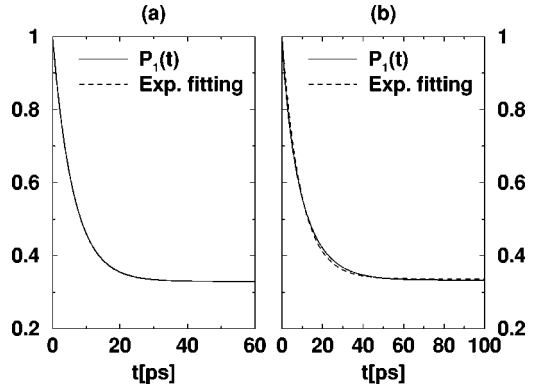

FIG. 2. Comparison between the numerical results for the evolution of the donor population, $P_1(t)$, (solid lines) and their single-exponential fitting curves (dashed lines) for two different values of the relaxation time τ. The parameter values are $\lambda_1 = 800\ \mathrm{cm}^{-1}$, $\lambda_2 = 200\ \mathrm{cm}^{-1}$, $\Delta = 20\ \mathrm{cm}^{-1}$, $T = 300$ K, (a) $\tau = 0.2$ ps and (b) $\tau = 2$ ps.

In Fig. 2 we show two typical numerical evolutions of $P_1(t)$ and their corresponding single-exponential fitting curves for a fixed value $\Delta = 20\ \mathrm{cm}^{-1}$ and two different values of the relaxation time (a) $\tau = 0.2$ ps and (b) $\tau = 2$ ps. Figure 2(a) demonstrates that the evolution is single exponential to a very good degree. The increase of τ by one order of magnitude [cf. Fig. 2(b)] introduces visible deviations from the strictly exponential behavior. In the following, we restrict our analysis to the case $\Delta \leqslant 10\ \mathrm{cm}^{-1}$ and $\tau \leqslant 2.5$ ps in order to ensure the strictly exponential character of the evolution.

In Figs. 3, 4, and 5 we depict the numerical and analytical results for a fixed value $\tau = 1$ ps and three different values of the tunneling matrix element, $\Delta = 1$, 5, and $10\ \mathrm{cm}^{-1}$, respectively. In the three figures we find an excellent agreement between the numerics and our analytical theory. In particular, for weak tunneling, $\Delta = 1\ \mathrm{cm}^{-1}$, the transfer is nonadiabatic and the numerical transfer rate Γ is perfectly reproduced by the nonadiabatic rate expression, Eqs. (38) and (40)–(42), in the whole range of the electronic energy bias ϵ_0 [cf. Fig. 3(a)]. When Δ increases, the nonadiabatic rate expression starts to fail [cf. Figs. 4(a) and 5(a)], especially in the vicinity of the decoupling point $\epsilon_0 = \epsilon_c$ of the two diabatic energy surfaces ($\epsilon_c \approx 266\ \mathrm{cm}^{-1}$ for the present parameters). Here, the adiabatic corrections due to the sluggish dynamics of the reaction coordinate become increasingly important as the nonadiabatic tunneling gets drastically accelerated. However, the numerical results are still pretty well reproduced by the consecutive step rate given in Eqs. (38), (59), (40)–(42), (53), and (57). This agreement holds only in the range $\epsilon_0 < \epsilon_c$, since for $\epsilon_0 \geqslant \epsilon_c$ the consecutive

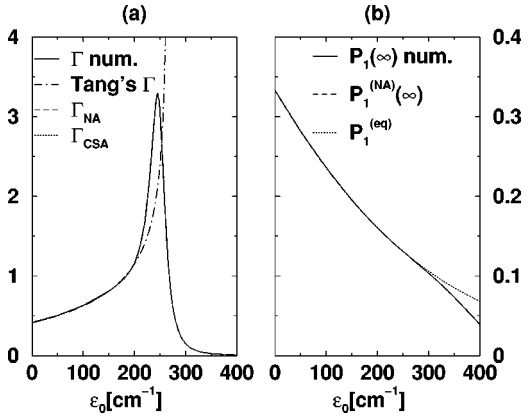

FIG. 3. (a) Dependence of the total rate constant (in ns^{-1}) on the energy bias ϵ_0 (in cm^{-1}). The numerical result is plotted with a solid line, the one obtained with Tang's approximation with a dash-dotted line, the nonadiabatic rate constant, $\Gamma_{NA}(\epsilon_0)$, with a dashed line, and the rate constant obtained, for $\epsilon_0<\epsilon_c$, from the consecutive step approximation, $\Gamma_{CSA}(\epsilon_0)$, with dotted line. (b) Dependence of the long-time population $P_1(\infty)$ on the energy bias ϵ_0 (in cm^{-1}). The numerical result is plotted with a solid line, the long-time population in the nonadiabatic limit with a dashed line, and the equilibrium result obtained from Eqs. (62) and (64) with a dotted line. In both panels the parameter values are $\lambda_1=800$ cm^{-1}, $\lambda_2=200$ cm^{-1}, $\Delta=1$ cm^{-1}, $T=300$ K and $\tau=1$ ps.

step approximation is not well defined. Notice that the rate values obtained with Tang's approximation (cf. the last paragraph in Sec. V B) depicted in Figs. 3(a), 4(a), and 5(a) significantly deviate from the numerics for $\epsilon_0 \gtrsim 200$ cm^{-1}.

One should also notice the strong asymmetry of the electron transfer rate against the inversion of the electronic bias $\epsilon_0 \rightarrow -\epsilon_0$ [cf. Figs. 4(a) and 5(a)]. This is in sharp contrast with the case of equal curvatures, where $\Gamma(-\epsilon_0)=\Gamma(\epsilon_0)$ (see, e.g., Fig. 7 in Ref. 21). Namely, in the present case $\Gamma(\epsilon_0)$ increases for positive ϵ_0 and exhibits a sharp maximum around $\epsilon_0 \sim \epsilon_c$. The origin of this maximum can be rationalized as follows. For a small Δ and neglecting the thermal dispersion of the reaction coordinate velocity v at the crossing point x^*, the probability $p(v)$ of the nonadiabatic tunneling transition between both curves is given by the Landau–Zener formula (see, e.g., Ref. 8)

$$p(v)=\frac{\pi\hbar\Delta^2}{|F_1-F_2|v}, \tag{61}$$

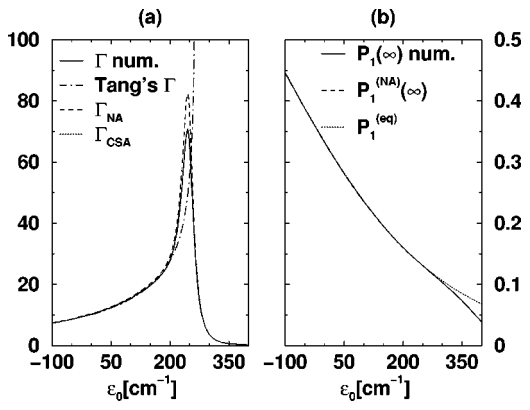

FIG. 4. The same as in Fig. 3 but with $\Delta=5$ cm^{-1}.

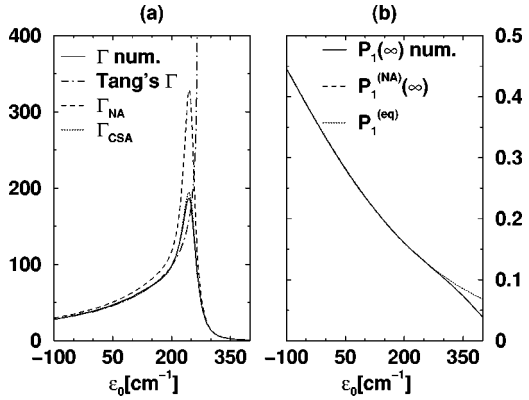

FIG. 5. The same as in Fig. 3 but with $\Delta=10$ cm^{-1}.

where $F_j=dV_j(x)/dx|_{x=x^*}$ are the slopes of the diabatic curves at the crossing point x^*. Even though this formula is valid only under the assumption that the diabatic curves can be considered, within the crossing region, as straight lines,[28] it provides a simple qualitative picture. Since $F_1=F_2$ when the two crossing points coalesce (cf. Fig. 1), the tunneling probability (61) exhibits a divergence that is responsible for the discussed sharp maximum. Averaging over the thermal distribution of v removes this divergence, but a sharp maximum remains and its position is shifted towards some smaller value $\epsilon_{max}<\epsilon_c$. Moreover, it turns out that the analytical values of Γ decay monotonically for negative values of ϵ_0 with an increase of $|\epsilon_0|$ (not shown). This latter result appears when the difference of the reorganization energies values is sufficiently large. For a small difference such a feature does not appear, but the discussed asymmetry is always present when $\lambda_1 \neq \lambda_2$.

The numerical and analytical dependences of the asymptotic population $P_1(\infty)$ on the energy bias ϵ_0 are shown in Figs. 3(b), 4(b), and 5(b). It is worth noting once more that the theoretical value of the asymptotic population does not depend on the adiabatic corrections, as it follows from Eq. (59). It is determined merely by the values of the nonadiabatic rate constants $k_{NA}^{(j)}$. Again, the agreement between the numerical and the theoretical values of $P_1(\infty)$ is almost perfect! Note that for zero energy bias $\epsilon_0=0$ the asymptotic population of the donor is less than one half, $P_1(\infty)<1/2$, and it remains so for small negative ϵ_0 [cf. Figs. 4(b) and 5(b)]. Thus, for such values of ϵ_0 the electron transfer occurs *against the electronic energy bias*. This effect, however, has nothing to do with a violation of the second law of thermodynamics, or a Maxwell demon effect. Its origin is due to the difference in the entropies of the reaction coordinate oscillator in the two different diabatic electronic states. Indeed, the relation between the thermal equilibrium populations of the two diabatic electronic states in the limit of very small electronic coupling, Δ, is given by

$$\frac{P_1^{(eq)}}{P_2^{(eq)}}=\exp\left(-\frac{G_1-G_2}{k_BT}\right). \tag{62}$$

In Eq. (62), G_j represents the free energy of a damped harmonic oscillator moving on the energy curve $V_j(x)$. In the

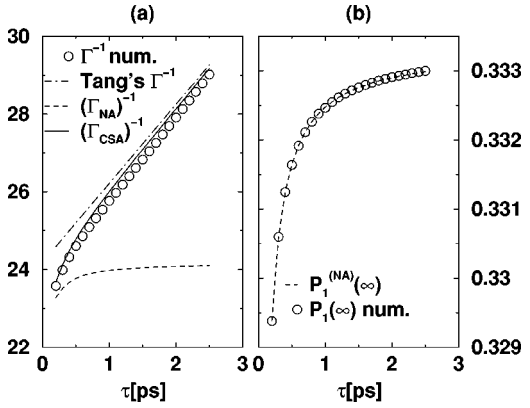

FIG. 6. (a) Dependence of the reciprocal of the rate constant Γ^{-1} (in ps) and (b) of the long-time population $P_1(\infty)$ on the solvent relaxation time τ (in ps). The numerical results are indicated with circles and those obtained from the nonadiabatic expressions with dashed lines. In (a) we have also plotted with solid line the rate constant obtained from the consecutive step approximation and with a dash-dotted line the one obtained with Tang's approximation. In both panels the parameter values are $\lambda_1=800$ cm^{-1}, $\lambda_2=200$ cm^{-1}, $\Delta=10$ cm^{-1}, $T=300$ K, and $\epsilon_0=0$.

semiclassical limit, the partition functions of the damped harmonic oscillator on each curve are given by[29]

$$Z_j^{(cl)}=\frac{k_BT}{\hbar\omega_j}\exp\left(\frac{\delta_{j,2}\,\epsilon_0}{k_BT}\right), \tag{63}$$

where the exponential factor is due to the vertical shift between the two minima of the harmonic potentials. Consequently, using the relation $G=-k_BT\ln Z$, the free energy difference in the semiclassical limit is

$$G_1-G_2=\epsilon_0-k_BT\,\ln\left(\frac{\omega_2}{\omega_1}\right)=\epsilon_0-\frac{1}{2}k_BT\,\ln\left(\frac{\lambda_2}{\lambda_1}\right), \tag{64}$$

where we have taken into account that $\lambda_j\propto\omega_j^2$. The term ϵ_0 on the right-hand side (r.h.s.) of Eq. (64) represents the change in internal energy, as can be easily checked from the relation $U=k_BT^2\partial\ln Z/\partial T$ between the internal energy, U, and the partition function. The second term corresponds to the entropic contribution to the free energy difference, $-T(S_1-S_2)$. Thus, a difference in reorganization energies between the backward and forward reactions yields an additional term of entropic origin in the free energy difference.

The equilibrium population $P_1^{(\mathrm{eq})}$ as obtained from Eqs. (62) and (64) is also depicted in Figs. 3(b), 4(b), and 5(b). For $\epsilon_0<\epsilon_c$, its values practically coincide with the long-time populations obtained from the numerical and analytical solutions of the Zusman equations. Thus, in this range of parameters, the long-time solutions of the Zusman equations are consistent with the principle of detailed balance in the semiclassical limit. However, for $\epsilon_0>\epsilon_c$, a significant discrepancy between the predictions of the Zusman equations and those of Eqs. (62) and (64) is observed. This fact may indicate a possible failure of the Zusman equations to describe properly the long-time populations for $\epsilon_0>\epsilon_c$, even for relatively small reorganization energies.

In Fig. 6, we show the dependence of the reciprocal of the total rate and the long-time population of the donor state on the solvent relaxation time τ, for a fixed value $\Delta=10$ cm^{-1} and zero electronic energy bias. As τ increases, the reciprocal of the rate constant is proportional to the relaxation time, $1/\Gamma\propto\tau$, in agreement with the analytical results. This indicates the transition to the solvent-controlled adiabatic regime.[6] Moreover, the agreement between the numerical and analytical values of the long-time population is almost perfect [cf. Fig. 6(b)]. Note that the corresponding values of $P_1(\infty)$ given by the Zusman equations depend on τ and slightly deviate from the thermal equilibrium value $P_1^{(eq)}=1/3$ given by Eqs. (62) and (64). This violation of the principle of detailed balance is very small indeed and the use of the Zusman equations is well justified. Especially, it is clearly seen from Fig. 6(b) that $P_1(\infty)$ approaches the correct equilibrium value obtained in the semiclassical limit when τ increases.

Finally, one should remark that the Zusman equations are thought to be difficult for numerical analysis. Indeed, in view of the several different time scales appearing in the problem, the corresponding system of ordinary linear differential equations obtained after discretization in space is stiff. This means that the corresponding minimal, $|\alpha_{\min}|$, and maximal, $|\alpha_{\max}|$, eigenvalues can be drastically different and the stiffness parameter, $\xi=|\alpha_{\max}|/|\alpha_{\min}|$, can be large. This seems to be source of numerical difficulties. For example, we have observed that the time spent by the NAG numerical routine to handle the numerical integration depends drastically on the parameters. In particular, for $\epsilon_0<0$ and the parameters used, the required computing time grows very quickly with $|\epsilon_0|$, perhaps exponentially. This is the practical reason why we do not have data in our figures for these values of ϵ_0. However, for $\epsilon_0>\epsilon_c$ we did not meet any numerical problem. The agreement between the numerical and the analytical results is very good. Thus, the deviation between the long-time populations obtained from the Zusman equations and the semiclassical thermodynamical result for $\epsilon_0>\epsilon_c$ is not due to numerical problems. The problem may be in the Zusman equations themselves, as in the case of large reorganization energies.[19] Nevertheless, these equations seem to be superior to other approximate semiclassical approaches for a rather broad range of parameters.[23]

VII. CONCLUDING REMARKS

In this paper, we have considered the extension of the Zusman equations to ET reactions in condensed media with different reorganization energies for the forward and backward reactions. The electron transfer process is assumed to be modeled by a set of partial differential equations describing the fluctuational relaxation of the reaction coordinate and the tunneling transitions between the electronic states. Using projection operator techniques and assuming appropriate initial conditions for the reduced density operator, we have proved that the populations of reactants and products satisfy a generalized master equation. The evaluation of the convolution kernels appearing in this equation entails the summation of a series whose terms depend on the diagonal and off-diagonal Green functions in a rather complicated way. A calculation of these Green functions has been carried out in the Appendixes. It should be pointed out that, to the best of

our knowledge, the expression of the off-diagonal Green function presented in this paper has not appeared previously in the literature.

From the above-mentioned exact, though formal, results we have obtained the following relevant information pertinent to ET kinetics: (i) We have provided a detailed discussion of the conditions under which the decay of the populations to their long-time values can be properly described by a single-exponential function for all the relevant time scales. Roughly speaking, this simple description is valid whenever there is a clear-cut separation between the relaxation time of the populations and those of the Green functions. (ii) We have obtained explicit expressions for the parameters characterizing the single-exponential decay, i.e., the long-time values of the populations, $P_j(\infty)$, and the total rate constant, Γ. As these formal expressions are rather complicated, we have resorted to approximations in order to simplify them. (iii) We have considered the nonadiabatic limit, i.e., we have assumed that Δ is the smallest energetic value involved in the reaction. In this limit we have provided a novel extension of the usual Marcus formula to the case of different curvatures. It should be pointed out that our formula does not rely on the use of the contact approximation as that proposed by Tang in Ref. 15. As noted in our previous work,[18] the contact approximation is untenable for some regions of the parameters space, leading to disagreements with the results obtained by numerical solution of the Zusman equations.[30] (iv) We have analyzed the kinetics beyond the nonadiabatic limit by using the consecutive step approximation. In this way, we have rigorously derived a novel expression for the total rate constant that allows us to describe both the nonadiabatic and the solvent-controlled adiabatic regimes. This expression is rather cumbersome but, under well-defined conditions, it can be cast in a form that constitutes the natural extension to the two curvatures case of the formula commonly used in the single curvature situation.[20,21] (v) A thorough comparison of the analytical predictions and the results obtained from the numerical solution of the Zusman equations has been carried out.

It should be noticed that, as we mentioned in the Introduction, in this paper we are accepting the validity of the Zusman equations. In Sec. VI, we have observed that there are situations where the validity of such a description is questionable. More precisely, for some parameter values, we have noticed deviations of the long-time populations predicted by the Zusman equations and those expected from statistical thermodynamical considerations in the semiclassical limit. In strongly polar solvents another kind of nonphysical predictions have been already pointed out by Frantsuzov.[19] Thus, even though the derivation of Zusman equations from a microscopic point of view has been repeatedly carried out in the literature,[20–23] the range of parameter values for which their validity is granted are not sufficiently well delimited.

ACKNOWLEDGMENTS

The authors gratefully acknowledge support of this work by Acciones Integradas (Grant 314/Al-e-dr; HA2001-0098) and (J. Casado-Pascual) by Grant No. A/01/19459 from DAAD. Support by the Dirección General de Enseñanza Superior of Spain (Project No. PB98-1120) is also acknowledged (J. C.-P. and M. M.).

APPENDIX A: GREEN FUNCTIONS FOR THE HARMONIC POTENTIALS WITH DIFFERENT CURVATURES

1. The off-diagonal Green function

In this Appendix we evaluate the off-diagonal Green function by solving the differential equation (11) with initial condition (12) and boundary conditions (13). After replacing the potentials (6) in Eq. (11), we obtain

$$\frac{\partial}{\partial t}G_{od}(x,t|x')=\left\{D\frac{\partial^2}{\partial x^2}+\frac{x_0}{\tau}\frac{\partial}{\partial x}\left(\frac{x}{x_0}-\frac{\lambda_2}{\lambda_1+\lambda_2}\right)-\frac{i}{\hbar}\left[\frac{(\lambda_1-\lambda_2)x^2}{x_0^2}+\frac{2\lambda_2 x}{x_0}+\epsilon_0-\lambda_2\right]\right\}\times G_{od}(x,t|x'), \tag{A1}$$

where τ is the phenomenological relaxation time of the overdamped oscillator on the averaged potential curve $[V_1(x)+V_2(x)]/2$ [cf. Eq. (8)]. The solution of Eq. (A1) is obtained by carrying out the Fourier transform with respect to x, i.e.,

$$\overline{G}_{od}(k,t|x')=\frac{1}{\sqrt{2\pi}}\int_{-\infty}^{\infty}dx\, e^{ikx}G_{od}(x,t|x'). \tag{A2}$$

The equation for the Fourier transform reads

$$\frac{\partial}{\partial t}\overline{G}_{od}(k,t|x')=\left\{-Dk^2+\frac{ikx_0}{\tau}\left(\frac{i}{x_0}\frac{\partial}{\partial k}+\frac{\lambda_2}{\lambda_1+\lambda_2}\right)+\frac{i}{\hbar}\left(\frac{\lambda_1-\lambda_2}{x_0^2}\frac{\partial^2}{\partial k^2}+\frac{2i\lambda_2}{x_0}\frac{\partial}{\partial k}-\epsilon_0+\lambda_2\right)\right\}\overline{G}_{od}(k,t|x'), \tag{A3}$$

which, except for $\lambda_1=\lambda_2$, is not simpler than Eq. (A1), as the second-order derivative still appears by contrast to the case of equal curvatures. Nonetheless, working in Fourier space is still convenient as further calculations are facilitated by the use of the initial condition

$$\overline{G}_{od}(k,0|x')=\frac{e^{ikx'}}{\sqrt{2\pi}}. \tag{A4}$$

Substitution of the ansatz

$$\overline{G}_{od}(k,t|x')=\frac{1}{\sqrt{2\pi}}\exp[-a(t,x')k^2-b(t,x')k-c(t,x')] \tag{A5}$$

in Eqs. (A3) yields the set of differential equations

$$\dot{a}(t,x')=D-\frac{2}{\tau}a(t,x')-\frac{4i(\lambda_1-\lambda_2)}{\hbar x_0^2}a^2(t,x'), \tag{A6}$$

$$\dot{b}(t,x') = -\left[\frac{1}{\tau} + \frac{4i(\lambda_1-\lambda_2)}{\hbar x_0^2}a(t,x')\right]b(t,x') - \frac{4\lambda_2}{\hbar x_0}a(t,x') - \frac{i\lambda_2 x_0}{(\lambda_1+\lambda_2)\tau}, \tag{A7}$$

$$\dot{c}(t,x') = \frac{i(\lambda_1-\lambda_2)}{\hbar x_0^2}[2a(t,x') - b^2(t,x')] - \frac{2\lambda_2}{\hbar x_0}b(t,x') + \frac{i(\epsilon_0-\lambda_2)}{\hbar}, \tag{A8}$$

which, according to Eqs. (A4) and (A5), has to be solved with the initial conditions $a(0,x')=c(0,x')=0$ and $b(0,x')=-ix'$. After some lengthy calculations and simplifications, one obtains

$$a(t,x') = a(t) = D\tau f_1(t), \tag{A9}$$

$$b(t,x') = -i\alpha x' f_0(t) - x_0\Lambda_2\left[if_1(t) + \frac{2(\chi+i)}{\alpha}f_2(t)\right], \tag{A10}$$

$$c(t,x') = \frac{i(\lambda_1-\lambda_2)\tau}{\hbar}f_1(t)\left(\frac{x'}{x_0}\right)^2 + \frac{2i\lambda_2\tau}{\hbar}\left[f_1(t) + \frac{4\Lambda_1}{\alpha}f_2(t)\right]\frac{x'}{x_0} - \frac{\lambda_2\Lambda_2\tau}{\hbar\alpha^2} \times \left\{[\chi+i(2\Lambda_1+1)]f_1(t) + \frac{8\Lambda_1(\chi+i)}{\alpha}f_2(t)\right\} + \left\{\frac{\lambda_2\Lambda_2[\chi+i(2\Lambda_1+1)]}{\hbar\alpha^2} - \frac{1}{2\tau} + \frac{i(\epsilon_0-\lambda_2)}{\hbar}\right\}t - \tfrac{1}{2}\ln[\alpha f_0(t)], \tag{A11}$$

where we have introduced the dimensionless parameters

$$\Lambda_j = \frac{\lambda_j}{\lambda_1+\lambda_2}, \tag{A12}$$

$$\chi = \frac{4k_BT\tau}{\hbar}, \tag{A13}$$

$$\alpha = [1+i(\Lambda_1-\Lambda_2)\chi]^{1/2}, \tag{A14}$$

and the functions

$$f_0(t) = \left[\sinh\left(\frac{\alpha t}{\tau}\right) + \alpha\cosh\left(\frac{\alpha t}{\tau}\right)\right]^{-1},$$

$$f_n(t) = f_0(t)\left[\sinh\left(\frac{\alpha t}{n\tau}\right)\right]^n \quad \text{for } n=1,2. \tag{A15}$$

Notice that the argument of the logarithm in Eq. (A11) is a complex function of the real variable t. Thus, for the function to vary continuously, we have to consider the Riemann surface where the infinite set of branches of the logarithmic function are defined. At $t=0$, the function starts at the main branch (i.e., the branch where $\ln 1=0$) and, as time increases, it goes over the next branches at each crossing of the cut in the complex plane. Transforming back to x space, one finds

$$G_{od}(x,t|x') = \frac{1}{2\sqrt{\pi a(t)}}\exp\left\{-\frac{[x-ib(t,x')]^2}{4a(t)} - c(t,x')\right\}. \tag{A16}$$

It is not difficult to prove that $\mathrm{Re}[a(t)]>0$ for $t>0$,[31] so that the boundary conditions (13) are obviously satisfied. This result for the off-diagonal Green function generalizes to the case of diabatic curves with different curvatures the one given in Ref. 21.

2. The diagonal Green functions

The evaluation of the diagonal Green functions for harmonic potential curves is straightforward. Substitution of the potential energies (6) in Eq. (16) yields the linear Fokker–Planck equation

$$\frac{\partial}{\partial t}G_d^{(j)}(x,t|x') = \left\{D\frac{\partial^2}{\partial x^2} + \frac{1}{\tau_j}\frac{\partial}{\partial x}(x-\delta_{j,2}x_0)\right\} \times G_d^{(j)}(x,t|x'), \tag{A17}$$

where τ_j is the phenomenological relaxation time of the overdamped oscillator on the potential curve $V_j(x)$ [cf. Eq. (7)]. By shifting x, Eq. (A17) is reduced to the forward Kolmogorov equation for the Ornstein–Uhlenbeck process.[32] Thus, $G_d^{(j)}(x,t|x')$ is obtained from the transition probability of the Ornstein–Uhlenbeck process by the substitutions $x \to x-\delta_{j,2}x_0$ and $x' \to x'-\delta_{j,2}x_0$, i.e.,

$$G_d^{(j)}(x,t|x') = \frac{1}{\sqrt{2\pi D\tau_j(1-e^{-2t/\tau_j})}} \times \exp\left\{-\frac{[x-\delta_{j,2}x_0-(x'-\delta_{j,2}x_0)e^{-t/\tau_j}]^2}{2D\tau_j(1-e^{-2t/\tau_j})}\right\}. \tag{A18}$$

APPENDIX B: EVALUATION OF THE SERIES IN EQ. (55)

In order to carry out the sum of the series (55), it is convenient to introduce two new auxiliary series, namely,

$$\nu_{j_1} = \sum_{n=1}^{\infty}\nu_{j_1}^{(n)} \quad \text{for } j_1=1 \text{ and } 2, \tag{B1}$$

where

$$\nu_{j_1}^{(1)} = r_{j_1}, \tag{B2}$$

$$\nu_{j_1}^{(n)} = (-1)^{n-1}r_{j_1}\sum_{j_2=1}^{2}\cdots\sum_{j_n=1}^{2}r_{j_2}\cdots r_{j_n}\prod_{l=2}^{n}\Xi_{j_{l-1},j_l} \tag{B3}$$

for $n\geqslant 2$. In the above expressions, we have simplified our notation by setting $\Xi_{j_{l-1},j_l} = \mathrm{Tr}[\tilde{\boldsymbol{k}}^{(1)}(0)\tilde{\boldsymbol{J}}(x_{j_{l-1}}^*,0|x_{j_l}^*)]$. Obviously, the series (55) can be obtained from the two series (B1) by $\nu = \Sigma_{j_1=1}^2\nu_{j_1}$.

The terms (B3) obey the recurrence relation

$$\nu_{j_1}^{(n)} = -r_{j_1} \sum_{j_2=1}^{2} \Xi_{j_1,j_2} \nu_{j_2}^{(n-1)}. \tag{B4}$$

Summing up the above expression from $n=2$ to ∞, one obtains after some rearrangements,

$$\sum_{j_2=1}^{2} [r_{j_1} \Xi_{j_1,j_2} + \delta_{j_1,j_2}] \nu_{j_2} = r_{j_1}. \tag{B5}$$

The above expression is a set of two (for $j_1=1$ and 2) linear equations in ν_{j_1}. Its solution is straightforward, yielding

$$\nu_{j_1} = \frac{r_{j_1} + r_1 r_2 \Sigma_{l=1}^{2} \Sigma_{m=1}^{2} (-1)^{l+m} (1-\delta_{j_1,l}) \Xi_{l,m}}{\Pi_{l=1}^{2} [1 + r_l \Xi_{l,l}] - r_1 r_2 [\Xi_{1,2}]^2}, \tag{B6}$$

where we have made use of the symmetry $\Xi_{1,2} = \Xi_{2,1}$. Finally, the sum of the series (55) is

$$\nu = \sum_{j_1=1}^{2} \nu_{j_1} = \frac{1 + r_1 r_2 \Sigma_{l=1}^{2} \Sigma_{m=1}^{2} (-1)^{l+m} \Xi_{l,m}}{\Pi_{l=1}^{2} [1 + r_l \Xi_{l,l}] - r_1 r_2 [\Xi_{1,2}]^2}. \tag{B7}$$

[1] *Electron Transfer: From Isolated Molecules to Biomolecules*, edited by J. Jortner and M. Bixon, Adv. Chem. Phys. **106** (Part I) (1999); **107** (Part II) (1999).
[2] A. V. Barzykin, P. A. Frantsuzov, K. Seki, and M. Tachiya, Adv. Chem. Phys. **123**, 511 (2002).
[3] R. A. Marcus, J. Chem. Phys. **24**, 966 (1956); **26**, 867 (1957); Discuss. Faraday Soc. **29**, 21 (1960).
[4] N. S. Hush, J. Chem. Phys. **28**, 962 (1958).
[5] V. G. Levich and R. R. Dogonadze, Dokl. Akad. Nauk SSSR **124**, 123 (1959) [Sov. Phys. Dokl. **124**, 9 (1959)].
[6] L. D. Zusman, Chem. Phys. **49**, 295 (1980).
[7] I. V. Alexandrov, Chem. Phys. **51**, 449 (1980).
[8] A. Garg, J. N. Onuchic, and V. Ambegaokar, J. Chem. Phys. **83**, 4491 (1985).
[9] T. Kakitani and N. Mataga, J. Phys. Chem. **89**, 4752 (1985).
[10] W. W. Parson, Z. T. Chu, and A. Warshel, Biophys. J. **74**, 182 (1998).
[11] C. Denk, M. Morillo, F. Sánchez-Burgos, and A. Sánchez, J. Chem. Phys. **110**, 473 (1999).
[12] P. Pérez-Tejada, F. J. Franco, A. Sánchez, M. Morillo, C. Denk, and F. Sánchez-Burgos, Phys. Chem. Chem. Phys. **3**, 1271 (2001).
[13] C. Hartnig and M. T. M. Koper, J. Chem. Phys. **115**, 8540 (2001).
[14] H.-X. Zhou and A. Szabo, J. Chem. Phys. **103**, 3481 (1995).
[15] J. Tang, Chem. Phys. **188**, 143 (1994).
[16] R. I. Cukier, J. Chem. Phys. **88**, 5594 (1988).
[17] M. Morillo and R. I. Cukier, J. Chem. Phys. **89**, 6736 (1989).
[18] J. Casado-Pascual, I. Goychuk, M. Morillo, and P. Hänggi, Chem. Phys. Lett. **360**, 333 (2002).
[19] P. A. Frantsuzov, J. Chem. Phys. **111**, 2075 (1999).
[20] D. Y. Yang and R. I. Cukier, J. Chem. Phys. **91**, 281 (1989).
[21] L. Hartmann, I. Goychuk, and P. Hänggi, J. Chem. Phys. **113**, 11159 (2000); *ibid.* **115**, 3969 (2001) (erratum).
[22] I. Goychuk, L. Hartmann, and P. Hänggi, Chem. Phys. **268**, 151 (2001).
[23] M. Thoss, H. Wang, and W. H. Miller, J. Chem. Phys. **115**, 2991 (2001).
[24] J. Cao and Y. Jung, J. Chem. Phys. **112**, 4716 (2000).
[25] M. Tachiya, J. Phys. Chem. **93**, 7050 (1989).
[26] I. S. Gradshteyn and I. M. Ryzhik, *Table of Integrals, Series, and Products* (Academic, New York, 1965).
[27] M. Abramowitz and I. A. Stegun, *Handbook of Mathematical Functions* (Dover, New York, 1972).
[28] E. E. Nikitin and S. Ya. Umanskii, *Theory of Slow Atomic Collision* (Springer, Berlin, 1984).
[29] U. Weiss, *Quantum Dissipative Systems*, 2nd ed. (World Scientific, Singapore, 1999).
[30] It should be noted, however, that our new results are only valid for sufficiently small reorganization energies. The use of Zusman equations beyond the contact approximation should thus be restricted to similar cases. On the other hand, the contact approximation results (Refs. 15 and 18) can be extrapolated onto the case of large reorganization energies. These earlier results are consistent with the detailed balance relation (for nonadiabatic to solvent controlled adiabatic ET) and do not yield such nonphysical features as negative reaction rates.
[31] Indeed, by formally solving the real part of Eq. (A6) in terms of $\mathrm{Im}[a(t)]$, one obtains
$\mathrm{Re}[a(t)] = D\int_0^t dt' \exp\{-\int_{t'}^t dt''[2/\tau - 8(\lambda_1-\lambda_2)\mathrm{Im}[a(t'')]/(\hbar x_0^2)]\}$,
which is obviously positive for $t>0$.
[32] P. Hänggi and H. Thomas, Phys. Rep. **88**, 207 (1982); N. G. van Kampen, *Stochastic Processes in Physics and Chemistry* (North-Holland, Amsterdam, 1992).